MOX–Report No. 02/2009

A couple ecological-hydrodynamic model for the spatial distribution of sessile aquatic species in thermally forced basins

Luca BONAVENTURA, Cristian BIOTTO, Astrid DECOENE, Lorenzo MARI, Edie MIGLIO

MOX, Dipartimento di Matematica "F. Brioschi"
Politecnico di Milano, Via Bonardi 9 - 20133 Milano (Italy)

mox@mate.polimi.it http://mox.polimi.it

A coupled ecological-hydrodynamic model for the spatial distribution of sessile aquatic species in thermally forced basins

Luca Bonaventura [♯], Cristian Biotto[♯] [*], Astrid Decoene[♯] [†]
Lorenzo Mari[*], Edie Miglio[♯]

December 22, 2008

[♯] MOX – Modellistica e Calcolo Scientifico
Dipartimento di Matematica "F. Brioschi"
Politecnico di Milano
via Bonardi 9, 20133 Milano, Italy
luca.bonaventura@polimi.it, edie.miglio@polimi.it

[*] Dipartimento di Elettronica e Informazione
Politecnico di Milano
Via Ponzio 34/5, 20133 Milano, Italy
mari@elet.polimi.it

Keywords: Ecological modelling, acquatic species, environmental hydrodynamics, baroclinic flows, semi-Lagrangian methods.

AMS Subject Classification: 92D25, 92D40, 92B99, 65M60, 86A05

Abstract

The life cycle of several sessile or highly sedentary aquatic species is characterized by a pelagic stage, during which propagules are dispersed by the water flow. As a consequence, hydrodynamics plays a crucial role in redistributing offspring, thus deeply influencing the spatiotemporal dynamics of such species. In this work, we describe an integrated modeling framework that allows the coupling of a minimal – yet biologically well founded – ecological model for population dynamics at the local scale to an efficient numerical model of three dimensional

[*]Presently at Imperial College, London, UK,
[†]Presently at Université Paris Sud, Paris, France

free surface flows in a thermally forced basin. The computed hydrodynamical fields are employed in a Lagrangian description of larval transport at the basin scale. The developed modeling framework has been applied to a realistic case study, namely the spread of an idealized aquatic sedentary population in Lake Garda, Italy. The analysis of this case study shows that the interplay between demography and hydrodynamics can produce complex spatiotemporal dynamics. Our results also evidence that larvae can travel over relatively long distances even in a closed basin. A sensitivity analysis of the model outcomes shows that both biological traits and external forcings may remarkably influence the evolution of diffusion patterns in space and time.

1 Introduction

One of the most important and challenging problems in population ecology is the understanding of the spatial dynamics of animal populations. This represents indeed a very complex task, since it requires the study of processes occurring at different spatial scales, ranging from local ones, such as birth and death processes, to non-local ones, such as dispersal processes [29]. A case of particular interest is represented by those aquatic species that are sessile or highly sedentary as adults, but have a pelagic stage at the beginning of their life cycle (e.g., mussels, corals, etc.; see [20, 13]). For these species, the redistribution of organisms between subsequent generations is almost exclusively operated by the water flow. In particular, currents determine the patterns of larval dispersal. Such patterns can be extremely complex, since they reflect the effects of the underlying hydrodynamics [3, 13, 42], and play a key role in determining long-term spatiotemporal population dynamics.

Both numerical simulations and measurements of dispersal ability have contributed to better understanding of some features of larval transport in marine and freshwater ecosystems [39, 10]. The outcomes of numerical models have been sometimes profitably compared to those of genetic models [18], elemental fingerprinting techniques [40] or *in situ* larval culturing [3]. Nevertheless, coupled ecological-hydrodynamic models are still needed in order to understand and forecast spatial population dynamics in a comprehensive way, as first clearly stated by [37]. Such models may in fact contribute to answering the basic questions concerning larval dispersal, i.e., where do larvae go and where do larvae come from [28]. Although questions of this kind could seem too simplistic, they correspond *de facto* to some of the most debated topics in the literature on larval dispersal, such as the estimation of the spatial scale over which larval transport occurs [12] and the debate on the relevance of self-recruitment (that is, the retention of larvae in their native site) on population dynamics at the basin scale [10, 12, 3]. A comprehensive understanding of spatiotemporal recruitment patterns is also required to face important applied issues, such as population management and the design of protected areas [20, 47, 13].

In this work, we develop an integrated modeling framework that combines a minimal, (yet ecologically well-founded) population model for the local demographic dynamics of a spatially structured sessile population, with a rigorous description of transport effects. In particular, we aim to describe long-term population dynamics. This actually represents a necessary condition for the understanding of the spatiotemporal patterns of population abundance at the basin scale. Remarkably, very few works have reported the results of long-term analyses in the context of larval dispersal. In point of fact, a recent literature survey [33] shows that just 5 on the 69 reviewed papers on fish recruitment in marine ecosystems were multigenerational (e.g., [36]; see also [6]). Moreover, most works devoted to the analysis of larval dispersal refer to marine ecosystems, while we specifically address the study of closed water bodies.

From a modeling perspective, larval dispersal is described here by a Lagrangian approach. The velocity fields used to evaluate larval trajectories are computed using the volume-conservative finite element model described in [32, 8] and extended in [5] to include baroclinic effects due to thermal forcing induced by solar radiation. The resulting coupled model is applied to a case study concerning the spread of an ideal sessile organism in Lake Garda, Italy. Although the case study is not tailored on a specific animal population, we consider thermal end environmental forcings (solar radiation, wind stress, etc.) that are specific for the basin under study.

The manuscript is organized as follows. In section 2 we describe the hydrodynamic model, while in section 3 some details are given on the numerical method employed for its solution. The solar radiation model is described in section 4, while the simple ecological model is presented in section 5. The main features of the case study are introduced in section 6. The model is first validated with respect to its capability of reproducing realistic temperature fields. The results of several simulations of larval spread in lake Garda are then presented and discussed. In section 7 some conclusions are drawn on the applicability of the present approach to other similar problems and further developments of the present model are discussed.

2 The hydrodynamic model

The hydrodynamical model used in this work is based on the Reynolds averaged equations for 3D free-surface baroclinic flows, derived under hydrostatic and Boussinesq assumptions. Baroclinic terms allow the model to account for pressure variations due to fluid density variations, while a realistic definition of thermodynamic forcings enables to estimate correctly the heat budget of the water basin. In the present work, fluid density variations responsible for the baroclinic component of fluid pressure are assumed to be dependent on temperature only. Other factors (such as water salinity) have been disregarded, thus limiting the applicability of the model to freshwater ecosystems.

The equations of the hydrodynamic model read as follows

$$\frac{Du}{Dt} = -g\frac{\partial \eta}{\partial x} - g\frac{\partial}{\partial x}\int_z^\eta \Delta\rho dz + \frac{\partial}{\partial x}\left(\nu_{Vh}\frac{\partial u}{\partial x}\right) + \frac{\partial}{\partial y}\left(\nu_{Vh}\frac{\partial u}{\partial y}\right) + \frac{\partial}{\partial z}\left(\nu_{Vv}\frac{\partial u}{\partial z}\right) + f_C v, \quad (1)$$

$$\frac{Dv}{Dt} = -g\frac{\partial \eta}{\partial y} - g\frac{\partial}{\partial y}\int_z^\eta \Delta\rho dz + \frac{\partial}{\partial x}\left(\nu_{Vh}\frac{\partial v}{\partial x}\right) + \frac{\partial}{\partial y}\left(\nu_{Vh}\frac{\partial v}{\partial y}\right) + \frac{\partial}{\partial z}\left(\nu_{Vv}\frac{\partial v}{\partial z}\right) - f_C u, \quad (2)$$

$$\frac{\partial \eta}{\partial t} + \frac{\partial}{\partial x}\int_{-h}^\eta u dz + \frac{\partial}{\partial y}\int_{-h}^\eta v dz = 0, \quad (3)$$

$$\frac{DT}{Dt} = \frac{\partial}{\partial x}\left(\nu_{Th}\frac{\partial T}{\partial x}\right) + \frac{\partial}{\partial y}\left(\nu_{Th}\frac{\partial T}{\partial y}\right) + \frac{\partial}{\partial z}\left(\nu_{Tv}\frac{\partial T}{\partial z}\right) + q, \quad (4)$$

$$\frac{\partial u}{\partial x} + \frac{\partial v}{\partial y} + \frac{\partial w}{\partial z} = 0. \quad (5)$$

Flow velocities along x, y and z directions are denoted by u, v and w, respectively. Water temperature and free surface elevations are denoted by T and η, while h, f_C and q denote the bottom depth, Coriolis parameter and the sum of all heat sources and sinks (to be described later in greater detail). In the present formulation, density is computed by the state equation

$$\rho = \rho_0[1 - \alpha_T(T - T_R)^2], \quad (6)$$

where T is the temperature expressed in Celsius degrees, $T_R = 4°\mathrm{C}$, $\alpha_T = 6.8 \cdot 10^{-6}$ K^{-2} and $\rho_0 = 1000$ kg m^{-3} is a reference density value, while the relative density variations are denoted by $\Delta\rho = (\rho - \rho_0)/\rho_0$. Atmospheric pressure gradients have been neglected, since only applications to relatively small basins will be considered. Also, the horizontal turbulent viscosity in the momentum and temperature diffusion has been considered negligible.

3 The numerical approximation method

The system of hydrodynamic equations (1)-(4) has been discretized by an extension of the semi-implicit and semi-Lagrangian numerical method proposed in [32], that is described in detail in [5]. Introducing a series of discrete time levels t^n that cover the total time interval $(0, T]$ with N timesteps of constant length

$\Delta t = t^{n+1} - t^n$, the semi-implicit time discretization can be written as

$$\frac{u^{n+1} - u^n(\mathbf{X})}{\Delta t} = -g\frac{\partial \eta^{n+\vartheta}}{\partial x} - g\frac{\partial}{\partial x}\int_z^{\eta^n} \Delta\rho^{n+\vartheta} dz + f_C u^n + \frac{\partial}{\partial x}\left(\nu_{Vh}^n \frac{\partial u^n}{\partial x}\right) + \frac{\partial}{\partial y}\left(\nu_{Vh}^n \frac{\partial u^n}{\partial y}\right) + \frac{\partial}{\partial z}\left(\nu_{Vv}^n \frac{\partial u^{n+\vartheta}}{\partial z}\right), \quad (7)$$

$$\frac{v^{n+1} - v^n(\mathbf{X})}{\Delta t} = -g\frac{\partial \eta^{n+\vartheta}}{\partial y} - g\frac{\partial}{\partial y}\int_z^{\eta^n} \Delta\rho^{n+\vartheta} dz - f_C u^n + \frac{\partial}{\partial x}\left(\nu_{Vh}^n \frac{\partial v^n}{\partial x}\right) + \frac{\partial}{\partial y}\left(\nu_{Vh}^n \frac{\partial v^n}{\partial y}\right) + \frac{\partial}{\partial z}\left(\nu_{Vv}^n \frac{\partial v^{n+\vartheta}}{\partial z}\right), \quad (8)$$

$$\frac{\eta^{n+1} - \eta^n}{\Delta t} + \frac{\partial}{\partial x}\int_{-h}^{\eta^n} u^{n+\vartheta} dz + \frac{\partial}{\partial y}\int_{-h}^{\eta^n} v^{n+\vartheta} dz = 0, \quad (9)$$

$$\frac{T^{n+1} - T^n(\mathbf{X})}{\Delta t} - \frac{\partial}{\partial x}\left(\nu_{Th}^n \frac{\partial T^n}{\partial x}\right) - \frac{\partial}{\partial y}\left(\nu_{Th}^n \frac{\partial T^n}{\partial y}\right) - \frac{\partial}{\partial z}\left(\nu_{Tv}^n \frac{\partial T^{n+\vartheta}}{\partial z}\right) = q^{n+\vartheta}, \quad (10)$$

$$\frac{\partial u^{n+1}}{\partial x} + \frac{\partial v^{n+1}}{\partial y} + \frac{\partial w^{n+1}}{\partial z} = 0, \quad (11)$$

Here, $n+\vartheta$ denotes time averaging of two subsequent time levels with averaging parameter ϑ, that should be taken in the interval $[1/2, 1]$ in order to guarantee stability of the Crank-Nicolson time discretization (see the relevant linear stability analysis in [7]). Furthermore, $\mathbf{X}$ denotes the foot of the Lagrangian trajectory reaching point (x, y, z) at time level t^{n+1}. Note that horizontal viscous terms and Coriolis terms have been discretized explicitly, since they do not imply severe stability restrictions on the computational meshes used in the present application. As for the spatial discretization, the (x, y) plane has been covered with an unstructured triangular mesh, while the z direction has been discretized in a suitable number of horizontal layers. Along the lines of [32], Raviart-Thomas elements of order 0 are used for the momentum equations, while $\mathbf{P}_0$ finite elements have been used for the free surface and temperature.

The temperature equation (4) is solved first, uncoupled from the momentum and free surface equations. As shown in (4), temperature advection is treated in a semi-Lagrangian fashion, employing respectively cubic and linear interpolations in the vertical and horizontal directions for the reconstruction step. The vertical turbulent viscosity term is discretized by a finite volume approach in space and by the Crank-Nicolson method in time. The computation of the heat fluxes due to solar radiation is described in detail in the next Section. Solution of the temperature equation yields an updated density value that is used to compute baroclinic gradients. After this step, the algorithm follows exactly [32]. The updated value of η^{n+1} is computed by solving a Helmholtz equation obtained by substitution of (1) and (2) in (4). Finally, the velocity field is updated. The

vertical velocity is then recovered from the incompressibility constraint. It is to be remarked that, due to the lack of full coupling between baroclinic gradients and momentum equations, the resulting time discretization is only conditionally stable with respect to internal gravity waves, while unconditional stability with respect to external gravity waves is guaranteed by the semi-implicit discretization of the free surface equation. No-flow boundary conditions are imposed at the lateral boundaries of the spatial domain, while bottom friction and wind drag formulae are used at the bottom and free surface, respectively.

4 Solar radiation forcing on the water basin

Modeling the heat fluxes at the surface of an enclosed water basin is essential to correctly reproduce the dynamics and thermal budget of the basin itself. Furthermore, a correct estimation of the water temperature is mandatory for the simulation of most biological processes. We will start by defining the various contributions to the heat flux at the surface of the water basin, while the modeling approach to the description of total heat sources within the basin will be discussed later on in this section. The total heat flux at the surface can be decomposed into shortwave radiation Q_{Oc}, longwave radiation Q_{Ol}, sensible heat exchange Q_l and evaporation heat flux Q_e. Each of these terms will now be discussed in detail.

The total incoming shortwave radiation flux at the surface is defined according to [30] as

$$Q_{Oc} = I_0(1 - 0.65C_n^2)(1 - R_s)a_t, \tag{12}$$

where I_0 is the intensity of the radiation that would reach the Earth's surface in absence of the atmosphere, C_n is a cloudiness dimensionless coefficient varying from 0 (clear sky) to 1 (completely cloudy sky), $a_t = 0.6 \div 0.7$ is the atmospheric attenuation term, which depends on soil reflectivity and on the content of water vapor in the atmosphere, and R_s is the albedo coefficient. Both I_0 and R_s are functions of the relative position with respect to the sun. Thus, they are time dependent and have to be updated at each time step of the numerical simulation.

The albedo coefficient can be defined as $R_s = a\,(\alpha)^{-b}$ [23], where α is the angle (measured in degrees) of the sun position with respect to the ground, while a and b are two cloudiness dependent coefficients defined as

	a	b
$C_n < 0.5$	2.2	0.97
$C_n > 0.5$	0.95	0.75

The incoming solar radiation at the surface is computed by taking into account the possible presence of mountains surrounding the lake, which implies that sun rays reach the water surface only when the sun inclination α is larger

than a critical value α_{cr}. Thus, one can define

$$I_0 = \begin{cases} 0 & \alpha < \alpha_{cr}, \\ I_{SC} E_0 \sin\alpha & \alpha > \alpha_{cr}. \end{cases} \tag{13}$$

Here, $I_{SC} = 1367\mathrm{Wm}^{-2}$ is the value of the solar constant given in [17], while E_0 is a correction term that accounts for the eccentricity of the Earth's elliptic orbit. In [25], the approximate formula

$$\begin{aligned} E_0 \quad &= 1.00011 + 0.034221\cos\Gamma + 0.00128\sin\Gamma \\ &+0.000719\cos 2\Gamma + 0.000077\sin 2\Gamma, \end{aligned} \tag{14}$$

is proposed, where $\Gamma = 2\pi(d_n - 1)/365$ and d_n denote the progressive number corresponding to the the position of the current simulation day in the year ($d_n = 1$ corresponding to January 1 and $d_n = 365$ to December 31). Finally, the solar angle α is defined by the formula

$$\sin\alpha = \sin\delta\sin\phi + \cos\delta\cos\phi\cos\omega, \tag{15}$$

where δ is the solar declination angle, defined as

$$\begin{aligned} \delta \quad = \quad & 0.006918 - 0.399912\cos\Gamma + 0.070257\sin\Gamma - 0.006758\cos 2\Gamma \\ & + 0.000907\sin 2\Gamma - 0.002697\cos 3\Gamma + 0.00148\sin 3\Gamma, \end{aligned} \tag{16}$$

ϕ is the geographic latitude and ω is an angular width varying linearly between $\omega_a = \arccos(-\tan\phi\tan\delta)$ and $-\omega_a$ in such a way that it is zero at noon.

As discussed in [24], the total longwave radiation Q_{Ol} is the difference between two contributions representing the incoming longwave radiation Q^i_{Ol} from the atmosphere to the water body and the outgoing longwave radiation Q^o_{Ol}, so that $Q_{Ol} = Q^i_{Ol} - Q^o_{Ol}$. These terms can be modeled as

$$Q^o_{Ol} = \varepsilon\sigma T_s^4 \tag{17}$$

and

$$Q^i_{Ol} = \varepsilon_{air}\sigma(1 + 0.17C_n^2)T_{air}^4(1 - R_t), \tag{18}$$

respectively. Here, $\varepsilon = 0.972$ and ε_{air} are the water and air emissivities, respectively, $\sigma = 5.669 \cdot 10^{-8}\mathrm{Wm}^{-2}\mathrm{K}^{-4}$ is Stefan-Boltzmann constant, T_s and T_{air} are water surface and air temperatures, and $R_t = 0.03$ is the value of the longwave reflection coefficient proposed in [23]. Air emissivity can be computed by the formula $\varepsilon_{air} = C_\varepsilon T_{air}^2$ [44], where $C_\varepsilon = 0.937 \cdot 10^{-5}\mathrm{K}^{-2}$.

The radiative flux Q_e due to evaporation is defined by the formula

$$Q_e = \rho L_w(a_w + b_w|\mathbf{W}|)(e_s(T_r) - e_s(T_s)) \tag{19}$$

proposed in [23], where $a_w = 4.18 \cdot 10^{-11}\mathrm{ms}^{-1}\mathrm{Pa}^{-1}$, $b_w = 0.95 \cdot 10^{-11}\mathrm{Pa}^{-1}$, L_w is the latent evaporation heat, e_s is the saturated vapor pressure and T_r the

dewpoint temperature. For the latent evaporation heat and the saturated vapor pressure we use the formulae given in [23], i.e.,

$$\begin{aligned} L_w &= 1000(2499 - 2.36\,T_s^\circ), \\ e_s(T_s^\circ) &= 2.171 \cdot 10^{10}\, e^{\left(\frac{-4157}{T_s^\circ + 239.09}\right)}, \end{aligned} \tag{20}$$

where T_s° is the water temperature at the surface expressed in Celsius.

The sensible heat flux Q_l is modelled as proposed in [24]:

$$Q_l = C_H c_{p\,air} \rho_{air} |\mathbf{W}| (T_{air} - T_s), \tag{21}$$

where $C_H = 1.4 \cdot 10^{-3}$ is the heat transfer coefficient at the height of 10m above the surface, $\mathbf{W}$ is the wind velocity at the same height and $c_{p\,air}$ is the constant pressure specific heat of air.

Following [23], longwave radiation, sensible heat and evaporation fluxes at the surface are considered to have an impact on the superficial water layer only. Therefore, their values - along with surface shortwave flux - are used to impose a Neumann boundary condition at the surface for the temperature equation. Shortwave radiation, instead, can be assumed to penetrate to a larger extent into the water column, depending on the water turbidity. This effect is modelled in [23] as

$$Q_{Oc}(z) = Q_{Oc}(0)\gamma e^{-\gamma(\eta - z)}, \qquad z < \eta \tag{22}$$

where $\gamma = 1.1 z_{DS}^{-0.73}$ and z_{DS} is the Secchi distance parameter, i.e., the smallest water depth at which a reference area disk is not visible from the surface. Thus, the total forcing term in the temperature equation for the interior of the water body (4) can be defined as

$$q = \frac{1}{\rho c_p} \frac{\partial\, Q_{Oc}}{\partial z}, \tag{23}$$

where c_p is the constant pressure specific heat.

5 The ecological model and its coupling to hydrodynamics

In this section we describe the coupled ecological-hydrodynamic model. Firstly, we discuss the features of the idealized species life cycle. Then we sketch the demographic model and the procedures employed to evaluate larval transport. Finally, we introduce the larval connectivity matrix, a tool that helps to describe the core features of larval dispersal in a synthetic way.

5.1 The species life cycle

For the sake of simplicity, we limit our analysis to the case of semelparous species, i.e., to species whose individuals reproduce once in their lifetime and then die.

We also assume that the reproductive season is as short as to be reasonably considered impulsive and that the sex ratio at birth and in the population is balanced. Although these hypotheses could seem too restrictive, they apply to a wide spectrum of populations and ecosystems, ranging from insects to mussels and from fish to plants (see, for instance, [34, 35]). Finally, we consider species in which adults are sessile or highly sedentary (e.g., because they live anchored to the bottom) while propagules (either eggs or larvae) are benthonic (i.e., they can be transported by the waterflow). Note that this is the typical case of several mussel, coral or reef fish species [20, 13].

Therefore, our reference life cycle can be outlined as follows:

- in each year t adult females (A_t) reproduce, generating eggs (E_t) with per capita net fertility f (hence $E_t = fA_t$), then die;
- a fraction σ_E of fertilized eggs survive and become larvae ($L_t = \sigma_E E_t$);
- larvae grow and are dispersed by the water flow;
- a fraction σ_L of larvae survive, settle and are recruited as adults in the next year/generation ($A_{t+1} = \sigma_L L_t$).

Note that some of the steps just summarized describe yearly processes taking place at the local scale (i.e., adult reproduction and larval settlement), while others refer to phenomena that occur on a short time scale but on a large (basin) spatial scale (i.e., larval transport). Also, it is worth noticing that in many natural populations, fertility and/or survival parameters may depend on population abundance (density dependence), thus providing a mechanism for the self-regulation of the population. Density dependence has important implications also in the context of larval recruitment (see, e.g., [13] and more references therein).

5.2 The local demographic model

A number of models accounting for density dependence can be found in the literature (see, for instance, [31, 21]). Here we consider one of the simplest and most used, the Beverton-Holt model [4], slightly modified as proposed in [21] in order to account for demographic fluctuations. This model was originally formalized to describe the dynamics of fish stocks and has already been used to link larval dispersal to recruitment dynamics in sessile aquatic population with a benthonic life stage (e.g., [26, 2, 6]). In the Beverton-Holt model, larval survival is supposed to decrease with larval abundance itself, thus $\sigma_L = \sigma(L_t)$. The mechanism behind this assumption is that settling larvae have to compete for limited resources (either nutrients or space, or both). From a mathematical perspective, this yields a simple nonlinear deterministic model in discrete time. At the local scale, the model is defined by the equation

$$A_{t+1} = \sigma_E \sigma(L_T) f A_t.$$

In this equation, larval survival is a decreasing function of larval abundance, i.e.,

$$\sigma(L_T) = \frac{\sigma_0}{(1+\beta L_t)^{\xi}},$$

where σ_0 is larval survival when the abundance of larvae is low, while β and ξ are two positive parameters describing the intensity of density dependence. For $\xi \leq 1$, the only solution admitted by the model is a stationary equilibrium corresponding to the carrying capacity of the habitat. For $\xi > 1$, the model can also display more complex dynamics, including periodic and chaotic fluctuations of population densities [21].

The effects of larval transport have not been considered so far. However, the demographic model just introduced can be suitably extended to cope with spatial processes due to transport. In particular, consider that in each discrete spatial location i the Beverton-Holt model can be written as

$$A^i_{t+1} = \frac{\sigma_0}{\left(1+\beta \mathcal{L}^i_t\right)^{\xi}} \mathcal{L}^i_t,$$

where $\mathcal{L}^i_t$ is the amount of larvae arriving at location i after dispersal. The value of $\mathcal{L}^i_t$ must then be estimated on the basis of the velocity fields produced by the hydrodynamic model already described. Not all the elements in the computational domain represent viable locations for the survival and growth of the population. Adverse conditions of illumination, temperature, pressure, flux velocity and/or substrate composition may prevent the establishment of local populations (see, e.g., [13]). In the present work, we will use depth and temperature as proxies for habitat viability. Therefore, we define a patch as viable if its mean depth is not greater than a threshold value d_{max} and its temperature during the spawning season is above T_{min}.

5.3 Evaluating larval transport

Larval transport by the water flow is modeled by a Lagrangian approach, which represents a common choice in the literature (e.g., [41]; see also [47, 13] and more references therein), since it provides a natural and accurate framework to describe the movement of the larvae. The fate of individual larvae is in fact deeply influenced by the different spatial trajectories they follow [22]. In our simple approach, we consider that dispersing larvae are passively transported by currents, i.e., that they are unable to swim, orient themselves or perform vertical migrations. Although this is quite a common assumption in the description of larval dispersal (e.g., [26, 1]), active movements can also play a remarkable role in determining the mean distance traveled by larvae [43, 12, 47, 13].

The Lagrangian approach requires the computation of the trajectories followed by single larvae (individual based model). A system of three ordinary differential equations is integrated numerically to determine the position of each propagule. While in the horizontal directions the propagule velocity is identical

to the velocity of the flow, the vertical velocity component w_p is assumed to be given by the sum $w_p = w_{flow} + w_{buoy}$, where w_{flow} is the flow velocity and w_{buoy} is the velocity induced by the buoyancy effect

$$g\frac{\rho - \rho_L}{\rho_L},$$

where g is the gravity constant, ρ is the water density and ρ_L is the density of larvae. Other effects could be included in the evaluation of larval trajectories may be introduced at this point (see [33] for a critical survey of the issues that do typically emerge in this context), but we do not explore this possibility here.

Suitable initial conditions (corresponding to the initial position of each particle) have to be specified in order to solve the previous system of differential equations. Specifically, in the first year of simulation the ecological model is initialized by picking the point in the spatial domain where larvae (or adult individuals) are first injected, while in the subsequent years the initialization is carried out reading stored data for adult abundance and computing the larval output due to a reproductive event. Then, for each active element (i.e., for each element with positive larval abundance) n_p Lagrangian particles are generated. The value of n_p should be proportional to the total larval output in each element, but this could make model simulations very time-consuming. In fact, species with very high fecundities would result in huge numbers of particles. In order to avoid this unpleasant effect, the number n_p of Lagrangian particles released in each active element has been kept constant (we typically used $n_p = 100$), and the information about the larval abundance in the patch from which larvae are dispersed has been stored in a label. Therefore, Lagrangian particles ultimately represent blobs of larvae whose abundance can be easily computed as the ratio between the total larval abundance of the native element and the number of released particles n_p. The initial position of each blob is assigned randomly within each active element.

The computation of the Lagrangian steps is accomplished by integrating the equations of motions for the propagules between 0 and a final time t_L, representing the mean duration of the larval stage (assumed here to be constant; see, e.g., [6, 1]). Technically, numerical integration has been carried out by means of a standard explicit Euler method. To preserve accuracy we used a much smaller time step (in general 60 s) than that used to solve the hydrodynamic model. At the end of the larval period we let propagules settle in the element corresponding to their current position, if the element is viable, otherwise we assume that larvae cannot settle and die. This corresponds to assuming that mature larvae are able to perform (small) vertical active movements (e.g., [6]). Since larvae also experience mortality due to density dependence, in viable patch we evaluate survival through the modified Beverton-Holt model described above. Adult densities in each spatial location can then be evaluated on the basis of the abundance of settled larvae (at the next year) again with the help of the ecological model.

In order to start the Lagrangian simulation, also initial data for the hydrodynamic fields should be determined by application of a data assimilation technique. However, since this study is more aimed at demonstrating the feasibility of our approach, and considering the small amount of available data for the case study analysed in section 6, we have simply initialised the model with a constant free surface value and zero velocity and run it for a sufficiently long start up period (in the case considered in section 6, one month) under realistic wind and solar forcing, in order to generate realistic hydrodynamical conditions. Once a realistic circulation is established, the Lagrangian particles are released. This complex set of operations constitutes a year in the life cycle of the aquatic species. Therefore, it has to be iterated several times to study long-term spatiotemporal population dynamics. The resulting algorithm can be outlined in this way:

1. `initialize the hydrodynamic model;`
2. `initialize the ecological model;`
3. `generate` n_p `Lagrangian particles for each active element and assign larval abundance to each particle;`
4. `perform Lagrangian steps;`
5. `evaluate larval survival and settling in viable elements;`
6. `store data for adults and repeat.`

5.4 The larval connectivity matrix

In the numerical experiments presented in section 6 the solar and wind forcing, although realistic, are indeed periodic and completely deterministic. Thus, if the hydrodynamics initialization process is carried out by a simple start up run as described above, a single run of the hydrodynamic component is sufficient to fully describe dispersal processes during a given year. If hydrodynamics and thermodynamic parameters are chosen with reference to a standard year and inter-annual variations of the environmental conditions are negligible, the results obtained for the reference year can then be extended to the years to come. In the reminder of this work we assume that these hypotheses are indeed acceptable for our case study area, thus allowing a significant reduction of the computational cost of a simulation that spans several species life cycles. For a given simulation scenario we perform a single numerical experiment, covering one larval spawning season, and derive the so-called larval connectivity matrix, which represents a powerful tool to understand the spatial relationships existing among patches (e.g., [2]; see also [12, 42]).

Connectivity matrices are a standard tool in graph theory [9] and are widely used also in the ecological context to describe dispersal in fragmented habitats

[46]. In particular, a connectivity matrix states which patches in the landscape are connected each other and what is the intensity of the connection. As such, the larval connectivity matrix C has the following structure:

$$C = \begin{bmatrix} c_{11} & c_{12} & \cdots & c_{1n_{el}} \\ c_{21} & \cdots & \cdots & \cdots \\ \vdots & \vdots & \vdots & \vdots \\ c_{n_{el}1} & \cdots & \cdots & c_{n_{el}n_{el}} \end{bmatrix},$$

in which the element c_{ji} represents the fraction of larvae that are generated in i and settle in j during one life cycle, while n_{el} is the number of elements used to resolve the spatial domain on the $(x-y)$ plain. Larval transport can thus be evaluated in this way:

$$\mathcal{L} = \sigma_L C \mathbf{L}, \tag{24}$$

where $\mathbf{L}$ and $\mathcal{L}$ represent larval abundance in each discrete location before and after transport, respectively.

Notice that evaluating a larval connectivity matrix by means of the algorithm described above is straightforward. This task basically requires that a new label, reporting the information concerning the element in which the trajectory was originated, be attributed to each particle. Afterwards, to simulate the spread of the species it is sufficient to perform steps 1-4 of the algorithm sketched above, with the third step slightly modified so that Lagrangian particles are released in all viable (and not only in all active) elements. Once the larval connectivity matrix has been estimated, the simulation algorithm can thus be rewritten as:

1. `initialize the ecological model;`
2. `estimate the effects of larval transport by means of the connectivity matrix;`
3. `evaluate larval survival and settling;`
4. `store data for adults and repeat.`

6 A case study: the spread of a sedentary species in lake Garda (Italy)

In this section we present some results obtained applying the previously described model to a realistic case study, namely the spread of an ideal sedentary species in Lake Garda (Italy). We first introduce the domain of the case study and report some details about the validation of the hydrodynamic model with respect to its ability of reproducing realistic temperature fields. Then, we describe model simulations and analyze the impact of hydrodynamics on the spatial dynamics of the population. Finally, we present a first model sensitivity analysis and discuss the robustness of the results.

6.1 Introduction to the case study area and model validation

Lake Garda is the largest Italian lake. It lies at 45 degree of latitude, with an extension of about 368 km^2 and a mean and maximum depth of 70 m and 350 m, respectively, as shown in Figure 1. In order to discretize the spatial domain for the purpose of performing model simulations, we use relatively coarse unstructured meshes with an approximate mesh size of 20 m. As for the vertical discretization, we use layers with different thicknesses, ranging between 5 m (close to the water surface) and 50 m (at the bottom of the water body). However, this is done only to reduce the computational cost in this first assessment of the coupled model performance and does not represent an intrinsic limitation of the approach. In [5], simulations with finer meshes were carried out for the hydrodynamic model only, along with a number of idealized baroclinic tests. Here, we only present results with realistic temperature forcing.

As for the environmental forcings, the effect of wind stress is incorporated into the model in a simple but realistic way, namely by considering a periodic wind forcing corresponding to the main two wind currents on the lake, the 'Peler' and 'Ora' winds. Peler wind blows southward on the upper portion of the lake from the early nighttime to late morning, approximately. It can reach a maximum speed of 15 ms^{-1}. Ora wind blows in the opposite direction in the early afternoon, reaching a speed of approximately 12 ms^{-1}.

The validation of the solar radiation model, together with its coupling to the hydrodynamic model, has been carried out by simulating one year of lake dynamics with typical solar radiation conditions. A simulation time step $\Delta t = 900$ s has been used, while the time averaging parameter is set to $\vartheta = 0.6$. The computed water temperature at the surface has been then averaged over the lake and monthly time averages of this quantity have been compared to the corresponding climatological maximum and minimum average temperatures. Results are reported in Figure 2, showing that the computed values are generally consistent with the climatological ones, although a slight overestimation occurs during summer months.

A comparison with measured data has also been carried out for the temperature field at a single time instant. More specifically, in Figure 3 the surface temperature on a typical September day is compared to the corresponding field as recovered by NOAA satellite measurements (data available on the website of the University of Bern, Switzerland). Although it should be noted that the color maps used in the two plots are not exactly the same, the general pattern of the computed temperature field is in good agreement with the measured values.

6.2 Simulation of species spread

The computed velocity fields can be used to evaluate the effects of hydrodynamics on the spatial redistribution of larvae and generate the spatiotemporal patterns of species spread into the lake, by repeated application of the connec-

Parameter	Value	Parameter	Value
σ_E	0.1	ρ_L	ρ
σ_0	0.1	t_L	7 [d]
f	1000	d_{max}	50 [m]
β	0.0001	T_{min}	0 [C]
ξ	1		

Table 1: Biological parameter values.

tivity matrix as described by formula (24). To start a model simulation all the parameters have to be specified. In particular, hydrodynamic and thermodynamic parameters have been set to fit the case of Lake Garda as described above, while the species demographic parameters have been set to the values reported in Table 1. Notice that T_{min} has been chosen so that temperature does not play a role in habitat viability, which is in this setting only dependent on depth. Furthermore, in this reference simulation the density of the larvae is taken to be equal to that of the water.

Figure 4 shows a typical example of model simulation. The species begins its spread close to Peschiera sul Garda (approximately marked by a black arrow in panel (a) of Figure 4) and in a few years it reaches the whole south basin of Lake Garda. For the parameter setting of Figure 4, population densities in each patch settle on a stationary value. This is obviously due to the introduction of a compensatory density dependence ($\xi = 1$). However, we observe that the population is not homogeneously distributed among all the viable patches of the lake. Specifically, the carrying capacity of each site can be not completely exploited due to recruitment limitations, i.e, because there are less settling larvae than larvae that are potentially allowed to settle. As already noticed by [2], both density dependence and recruitment limitation can thus play a role in determining population dynamics. Therefore, both demographic processes and transport phenomena due to hydrodynamics are important to understand the evolution of spatiotemporal population patterns. As such, they should always be analyzed together in long-term studies.

Experiments of this kind can help answering some of the basic questions set in section 1, namely where do larvae go, or where do they come from [28]. Key to the understanding of such questions is the larval connectivity matrix C (Figure 5, panel (a), inset). In fact, by definition, the i-th column of C determines what is the fraction of larvae starting from patch i and arriving in patch j. In the same way, it is also possible to estimate where do larvae come from by just reading the rows of C. It may help to display the connectivity matrix in a spatially explicit setting. Figure 5(a) shows the strongest connections among patches

defined by matrix C ($c_{ij} > 0.05$, corresponding to the black dots in the sparsity plot reported in the inset). Interestingly, relatively few patches are characterized by several of such connections, while most patches seem to be poorly connected. Also, it turns out that the strongest links between patches occur among rather distant locations.

The larval connectivity matrix can be also used to evaluate the so-called dispersal kernel [45], which states what is the fraction of propagules that is expected to travel a given distance from the release point as a function of the distance from the native patch itself. Although dispersal kernels are usually rigorously defined for isotropic environments (in which dispersal is not affected by spatial dishomogeneity), they are often estimated also in cases in which the hypothesis of spatial homogeneity is violated, as in the case of larval transport [41, 43]. Figure 5(b) displays the mean dispersal kernel (i.e., the average of the dispersal kernels estimated with reference to each viable site in Lake Garda) for the scenario depicted in Figure 4. The inset shows the dispersal kernel obtained by excluding the effects of self-recruitment, i.e., by excluding larvae that settle in the same patch in which they have been released. As such, the kernel in the inset describes the probability that a propagule travels a given distance, provided that it leaves the native patch. Three regions can be identified in the dispersal kernel, respectively corresponding to short-, medium- and long-distance dispersal. Quite interestingly, more than 40% of the larvae do not move beyond 1 km (10% excluding self-recruitment) from the native element (short-distance dispersal), while more than 9% (13% if self-recruitment is disregarded) are dispersed for more than 10 km, approximately three times (long-distance dispersal) the distance traveled by larvae on average (about 3629 m). Note that such long-distance dispersal events may be very important in the maintenance of the population at the basin scale [10, 27, 11, 12].

The larval dispersal kernel is a very useful tool, since it helps summarizing the core characteristics of larval dispersal in the basin. However, some features of larval dispersal are highly site-dependent. In particular, both self-recruitment (i.e., the local retention of larvae in their native patch, corresponding to the main diagonal of C; Figure 5, panel (c)) and the mean distance traveled by larvae (d) vary remarkably among patches (as found in empirical observations; e.g., [12, 13]). The importance of self-recruitment represents another highly debated topic in the literature on larval dispersal [10, 12, 28, 3]. Simple statistical analyses show that in the scenario of Figure 4 the mean fraction of larvae being locally retained in each viable element is about 31.27% (variance 12.06%). We remark that estimating local larval retention can give important cues on the planning of management policies (e.g., in the case of invasive alien species or marine protected areas; e.g., [20, 47, 13]), specifically suggesting an *a priori* estimation of the potential effectiveness of control actions planned at the local/basin scale. A visual inspection of the bottom panels of Figure 5 shows that patches with low self-recruitment are typically characterized by short mean dispersal distances, and viceversa, with some notable exceptions close to the south-eastern coasts of

Lake Garda. We also remark that contrasting panels (c) and (d) of Figure 5 to panel (a) yields a better understanding of the structure of larval connectivity patterns, specifically defining larval sources and sinks [6].

6.3 Sensitivity analysis

The results of model simulations do obviously depend upon the specific parameter setting considered. Therefore, it is important to perform a sensitivity analysis of the model outcomes with respect to changes in the parameter values. Before presenting the results of this sensitivity study, it is to be remarked that model outcomes are also influenced by factors other than demographic, biological or thermodynamic parameters. Specifically, the spatial resolution at which the model analysis is carried out can have a significant impact on model outcomes. In our analyses, we have used a grid of 1593 elements and about 20 vertical layers with thickness varying between 5 (close to the surface) and 50 m (close to the bottom). This vertical discretization turned out to be an acceptable trade-off between the accuracy of the results and the efficiency of the computational scheme. Simulations with a coarser vertical discretization lead in fact to inaccuracies in the computation of velocity fields. Other parameter values, such as the number n_p of Lagrangian particles released from each element, can of course have an impact on model outcomes. For instance, we have run model simulations using $n_p = 50$ instead of $n_p = 100$ and found that in this way the spread of the species is remarkably underestimated.

The first type of analysis we present concerns the role of the demographic parameters σ_0, which quantifies survival from the larval stage to the adult phase (i.e., survival during transport and after settlement), and ξ, which describes the intensity of density dependence. Demographic parameters can have a strong impact on the densities reached by local colonies. For instance, higher σ_0's do obviously lead to more abundant local populations (panels (a) and (b) of Figure 6). As already remarked above, the densities reached by local colonies are highly site-dependent. As an example, population densities in Desenzano sul Garda (dots) are much lower than those recorded in Bardolino (diamonds). However, different values of the biological parameters σ_0 and ξ do not appear to alter the structure of the larval connectivity matrix C. Therefore, the long-term spatial pattern of species spreading remains qualitatively unaltered. On the other hand, increasing values of either σ_0 or ξ (or both) lead to interesting outcomes at the local scale. Local populations may in fact display wide demographic fluctuations. Such fluctuations can be either regular (periodic dynamics, Figure 6(c)) or highly irregular (chaotic dynamics, Figure 6(d)) and result from the introduction of an overcompensatory density dependence ($\xi > 1$). Therefore, this typical feature of the modified Beverton-Holt model [21] is still preserved when ecology and hydrodynamics are coupled. Quite interestingly, we observe that different spatial locations are in general characterized by different population densities averaged over time. Specifically, mean population densities in

Desenzano sul Garda are higher than those in Bardolino in case of periodic dynamics (Figure 6(c)). Also, notice that demographic fluctuations under periodic regime can be characterized by very different oscillation amplitudes and can be desynchronized [15, 14]. Years with high population densities in Desenzano sul Garda correspond in fact to years with low densities in Bardolino.

On the other hand, some other biologic parameters may influence the structure of the connectivity matrix C. This is the case, for instance, of larval density ρ_L. This result should be obviously expected: in fact, if ρ_L is greater than water density, then the vertical acceleration due to gravity becomes active and forces larvae towards the floor of the lake. As a result, propagules travel shorter distances than in the case in which $\rho_L = \rho$. However, this does not necessarily imply negative impacts on the spread of the species. Top panels of Figure 7 show what is expected to happen for small positive variations of larval density (on the order of 0.1% of water density). Although the mean distance traveled by dispersing larvae turns out to be shorter than in the previously analyzed scenario (2902 m), the spread of the species can be even promoted. Notice in fact that in this simulation scenario the species is expected to establish with high population densities also along the southern coasts of Lake Garda. This seemingly paradox can be explained by the observation than the closer a larva is dispersed (clearly from a viable patch), the higher the probability it can settle in a viable patch. Small positive variations of larval densities may thus mitigate recruitment limitations in otherwise poorly connected sites. However larger values of ρ_L do obviously reduce the spread of the species in a remarkable way. As an example, bottom panels of Figure 7 report the results of a simulation obtained with a larger positive variations of larval density with respect to water density (on the order of 1 %). In this case, larvae travel remarkably shorter distances (995 m) and the spread of the species is limited to the south-western part of the lake.

Water temperature plays an important role in the spread of aquatic species in several ways (see e.g., [13] and references therein). For instance, spawning is often regulated by temperature, meaning that the release of propagules cannot happen below a given temperature threshold. Also the duration of the larval phase may depend on temperature, as well as other demographic parameters such as larval survival or adult fertility. Top panels of Figure 8 show a model simulation in which the aquatic species is supposed to be sensitive to temperature. Specifically, we assume that a patch is viable for the population only if the mean temperature during the spawning season exceeds a minimum value $T_{min} = 10$ C and the mean depth does not exceed $d_{max} = 50$ m, as in the previous model runs. This assumption does obviously change connectivity patterns. A comparison between the top panels of Figure 8 and the bottom panels of Figure 4 shows that, although the stationary population distribution turns out to be quite similar in the two simulation scenarios, transient spatiotemporal dynamics can be quite different, mainly due to density dependence. A decrease in the number of viable patches leads in fact to a smaller abundance of both

released and settling larvae, which then experience higher survival rates, thus promoting a faster population growth. Temperature has also a direct influence on water flows and currents. As such, variations of mean and maximum temperature values used in thermal forcing terms can modify water circulation in the water body, thus altering larval redistribution patterns. As an example, bottom panels of Figure 8 show what happens in a scenario in which mean and maximum temperatures used in thermal forcing terms are 2 C higher. As already recorded in the previous simulation, the interplay between density-dependent demographic dynamics and hydrodynamics effects may produce nontrivial effects on the spatiotemporal evolution of the spread. This suggests that climate change may have a remarkable influence on spatiotemporal invasion patterns [16, 38, 13].

We finally remark that the visual inspection of the spatiotemporal patterns of population density can by no means be considered a formal tool to compare larval connectivity patterns. Quantitative comparison of the different connectivity matrices can highlight similarities and differences in larval dispersal (e.g., [13, 42]). A more synthetic way to estimate the impact of different simulation scenarios on the spatiotemporal evolution of the species spreading is the comparison of the singular values (see e.g. [19]) of the connectivity matrices evaluated with the help of the larval transport model, displayed in Figure 9. We note that both larval density (dashed line) and sensitivity to temperature (dash-dotted line) have a remarkable impact on the structure of larval connectivity (the solid line represents the singular values of the baseline case of Figure 4), even if they do not change water flows in Lake Garda. On the contrary, a small variation of the thermal forcings (dotted line) produces a less notable effect on the structure of the connectivity matrix. A general result is that connectivity patterns cannot be explained on the basis of few components of the matrix. As such, simplified box models cannot be successfully applied to analyze the problem at hand and sufficiently high resolution models are thus required to fully understand spatiotemporal population dynamics in Lake Garda.

7 Discussion and conclusions

In this work we have shown how a simple ecological model for the local demographic dynamics of a sedentary aquatic species can be coupled to a realistic description of the transport effects at the basin scale, in order to study the long-term dynamics of the population in a closed, thermally forced water body. Studying the evolution of these spatiotemporal patterns is a very complex task, which requires an integrated and highly interdisciplinary approach. However, understanding the patterns of species spread is mandatory in both conservation and management problems.

We have described local demographic dynamics by means of a modified Beverton-Holt model. The underlying hydrodynamic model implements a semi-

implicit and semi-Lagrangian method, thus ensuring efficiency and accuracy. Moreover, the introduction of realistic thermal end environmental forcing (solar radiation, wind stress, etc.) has allowed to link the hydrodynamics to a range of key biological processes. As for larval transport, a Lagrangian approach was used for evaluating larval trajectories. In addition, under some reasonable simplifying hypotheses, less costly long-term model simulations were achieved by estimation of the larval connectivity matrix, that allowed off-line computation of hydrodynamical effects on larval circulation. While analyzing a realistic case study (the spread of an ideal sedentary aquatic species in Lake Garda, Italy) we have found that although transport and retention effects are extremely site-dependent, larvae can generally travel over relatively long distances. Long-distance dispersal represents about 10% of total dispersal, thus possibly representing a key feature for the definition of the population dynamics at the basin scale. A sensitivity analysis of the model has shown that both biological parameters and thermal forcing can play a major role in determining long-term demographic dynamics, as well as the spatial distribution of the population.

Future developments of this work will concern the use of more realistic ecological models, a more thorough validation of the hydrodynamic component and the use of higher spatial resolutions. Also, the description of larval transport can be made more accurate by introducing some realistic details such as the possibility of swimming or performing oriented vertical migrations. All these improvements should be then validated against field data with the aim of producing an accurate (yet agile) model for analyzing complex spread problems in aquatic ecosystems.

Acknowledgments

The authors thank Marino Gatto, Renato Casagrandi (Politecnico di Milano) and Giulio de Leo (Università degli Studi di Parma) for useful comments and hints. A first version of the solar radiation model was developed by Dr. Giuliano Rizzi in his Master Thesis in Environmental Engineering (University of Trento, 1998). Finally, an essential input for this work was the encouragement and support we all received from Fausto Saleri, who initially planned and tutored the thesis of Cristian Biotto.

References

[1] C. M. Aiken, S. A. Navarrete, M. I. Castillo, and J. C. Castilla. Along-shore larval dispersal kernels in a numerical ocean model of the central Chilean coast. *Marine Ecology Progress Series*, 339:13–24, 2007.

[2] P. R. Armsworth. Recruitment limitation, population regulation, and larval connectivity in reef fish metapopulations. *Ecology*, 83:2093–1104, 2002.

[3] B. J. Becker, L. A. Levin, F. J. Fodrie, and P. A. McMillan. Complex larval connectivity patterns among marine invertebrate populations. *PNAS*, 104:3267–3272, 2007.

[4] R. Beverton and S. Holt. *On the Dynamics of Exploited Fish Populations*. H.M. Stationery Office, London, London, 1957.

[5] C. Biotto. Un modello numerico semi-implicito e semi-lagrangiano per fluidi a superficie libera con forzanti termiche: validazione e applicazioni alla fluidodinamica ambientale, 2007. Master thesis, Politecnico di Milano.

[6] M. Bode, L. Bode, and P. R. Armsworth. Larval dispersal reveals regional sources and sinks in the Great Barrier Reef. *Marine Ecology Progress Series*, 308:17–35, 2006.

[7] V. Casulli and E. Cattani. Stability, accuracy and efficiency of a semi-implicit method for three-dimensional shallow water flow. *Computers and Mathematics with applications*, 27(4):99–112, 1994.

[8] P. Causin and E. Miglio. Parallel computing for the simulation of 3D free surface flows in environmental applications. *Lecture Notes in Computer Science*, 2474:78–87, 2002.

[9] G. Chartrand. *Introductory Graph Theory*. Dover, New York, 1985.

[10] R. K. Cowen, K. M. M. Lwiza, S. Sponaugle, C. B. Paris, and B. D. Olson. Connectivity of marine populations: open or closed? *Science*, 287:857–859, 2000.

[11] R. K. Cowen, C. B. Paris, D. B. Olson, and J. L. Fortuna. The role of long distance dispersal versus local retention in replenishing marine populations. *Gulf and Caribbean Research*, 14:129–137, 2003.

[12] R. K. Cowen, C. B. Paris, and A. Srinivasan. Scaling of connectivity in marine populations. *Science*, 311:522–527, 2006.

[13] R. K. Cowen and S. Sponaugle. Larval dispersal and marine population connectivity. *Annual Review of Marine Sciences*, 1:443–466, 2009.

[14] D. J. Earn and S. A. Levin. Global asymptotic coherence in discrete dynamical systems. *Proceedings of the National Academy of Sciences USA*, 103:3968–3971, 2006.

[15] D. J. Earn, S. A. Levin, and P. Rohani. Coherence and conservation. *Science*, 290:1360–1364, 2000.

[16] P. A. Fields, J. B. Graham, R. H. Rosenblatt, and G. N. Somero. Effects of expected global climate change on marine faunas. *Trends in Ecology and Evolution*, 8:361–367, 1993.

[17] C. Fröhlich and R.W. Brusa. Solar radiation and its variation in time. *Solar Physics*, 74(1):209–215, 1981.

[18] H. M. Galindo, D. B. Olson, and S. R. Palumbi. Seascape genetics: A coupled oceanographic-genetic model predicts population structure of caribbean corals. *Current Biology*, 16:1622–1626, 2006.

[19] G.H. Golub and C.F. Van Loan. *Matrix Computations, 2nd edition*. The Johns Hopkins University Press, Baltimore, 1989.

[20] F. Guichard, S. A. Levin, A. Hastings, and D. Siegel. Toward a dynamic metacommunity approach to marine reserve theory. *BioScience*, 54:1003–1011, 2004.

[21] M. P. Hassell. Density-dependence in single-species populations. *Journal of Animal Ecology*, 44:283–295, 1975.

[22] M. R. Heath and A. Gallego. From the biology of the individual to the dynamics of the population. *Journal of Fish Biology*, 51:1–29, 1997.

[23] B. Henderson-Sellers. Calculating the surface energy balance for lake and reservois modelling: a review. *Reviews of Geophysics*, 24(3):625–649, 1986.

[24] J. Imberger and J.C. Patterson. *Transport Models for Inland and Coastal Waters*, chapter A dynamic reservoir simulation model - DYRESM: 5, pages 310–361. H.B. Fischer, Academic Press, 1981.

[25] M. Iqbal. *An introduction to solar radiation*. Academic Press Canada, 1983.

[26] M. K. James, P. R. Armsworth amd L. B. Mason, and L. Bode. The structure of reef fish metapopulations: modelling larval dispersal and retention patterns. *Proceedings of the Royal Society of London B*, 269:2079–2086, 2002.

[27] C. E. Kraft, P. J. Sullivan, A. Y. Karateyev, L. E. Burlakova, J. C. Nekola, L. E. Johnson, and D. K. Padilla. Landscape patterns of an aquatic invader: assessing dispersal extent from spatial distributions. *Ecological Applications*, 12:749–759, 2002.

[28] L. A. Levin. Recent progress in understanding larval dispersal: new directions and digressions. *Integrative and Comparative Biology*, 46:282–297, 2006.

[29] S. A. Levin. The problem of pattern and scale in ecology. *Ecology*, 73:1943–1967, 1992.

[30] J.L. Martin and S.C. McCutcheon. *Hydrodynamics and transport for water quality modeling*. Lewis Publishers, U.S., 1999.

[31] R. M. May. Biological population with non-overlapping generations: Stable points, stable cycles and chaos. *Science*, 186:645–647, 1974.

[32] E. Miglio, A. Quarteroni, and F. Saleri. Finite element approximation of Quasi-3D shallow water equations. *Computer Methods in Applied Mechanics and Engineering*, 174:355–369, 1999.

[33] T. J. Miller. Contribution of individual-based coupled physicalbiological models to understanding recruitment in marine fish populations. *Marine Ecology Process Series*, 347:127–138, 2007.

[34] E. C. Pielou. *Mathematical Ecology*. Wiley, 1977.

[35] R. E. Ricklefs and G. L. Miller. *Ecology*. W. H. Freeman and company, New York, 1999.

[36] K. A. Rose, C. A. Murphy, S. L. Diamond, L. Fuiman, and P. Thomas. Using nested models and laboratory data for predicting population effects of contaminants on fish: a step toward a bottom-up approach for establishing causality in field studies. *Human Ecology Risk Assessment*, 9:231–257, 2003.

[37] J. Roughgarden, S. Gaines, and H. P. Possingham. Recruitment dynamics in complex life cycles. *Science*, 241:1460–1466, 1988.

[38] K. Roy, D. Jablonski, and J. Valentine. Climate change, species range limits and body size in marine bivalves. *Ecology Letters*, 4:366–370, 2001.

[39] P. W. Sammarco and J. C. Andrews. Localized dispersal and recruitment in Great Barrier Reef corals: the Helix Experiment. *Science*, 239:1422–1424, 1988.

[40] T. M. Shank1 and K. M. Halanych. Toward a mechanistic understanding of larval dispersal: insights from genomic fingerprinting of the deep-sea hydrothermal vent tubeworm *Riftia pachyptila*. *Marine Ecology*, 28:25–35, 2007.

[41] D. A. Siegel, B. P. Kinlan, B. Gaylord, and S. D. Gaines. Lagrangian descriptions of marine larval dispersion. *Marine Ecology. Progress Series*, 260:83–96, 2003.

[42] D. A. Siegel, S. Mitarai, C. J. Costello, S. D. Gaines, B. E. Kendall, R. R. Warner, and K. B. Winters. The stochastic nature of larval connectivity among nearshore marine populations. *Proceedings of the National Academy of Sciences USA*, 105:8974–8979, 2008.

[43] R. S. Steneck. Staying connected in a turbulent world. *Science*, 311:480–481, 2006.

[44] W.C. Swinbank. Longwave radiation from clear skies. *Quarterly Journal Royal Meteorological Society*, 89:339–448, 1963.

[45] P. Turchin. *Quantitative Analysis of Movement*. Sinauer Associates, Sunderland, UK, 1998.

[46] D. Urban and T. Keitt. Landscape connectivity: A graph-theoretic perspective. *Ecology*, 82:1205–1218, 2001.

[47] F. E. Werner, R. K. Cowen, and C. B. Paris. Coupled biological and physical models. *Oceanography*, 20:54–69, 2007.

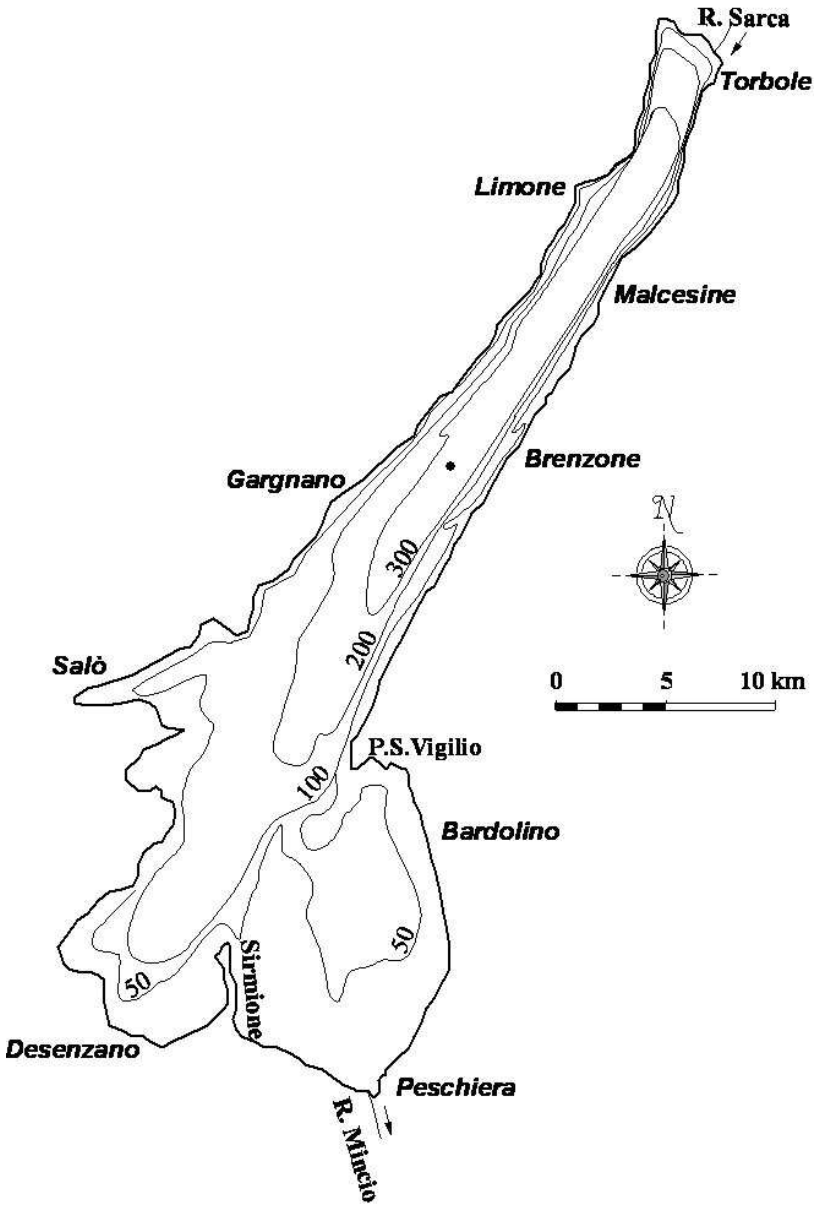

Figure 1: Bathymetry of Lake Garda

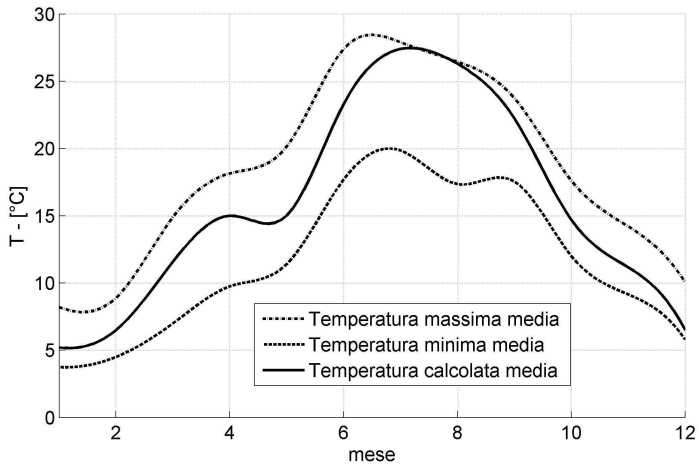

Figure 2: Monthly averaged temperature obtained in a year long simulation compared to climatological maximum and minimum temperatures.

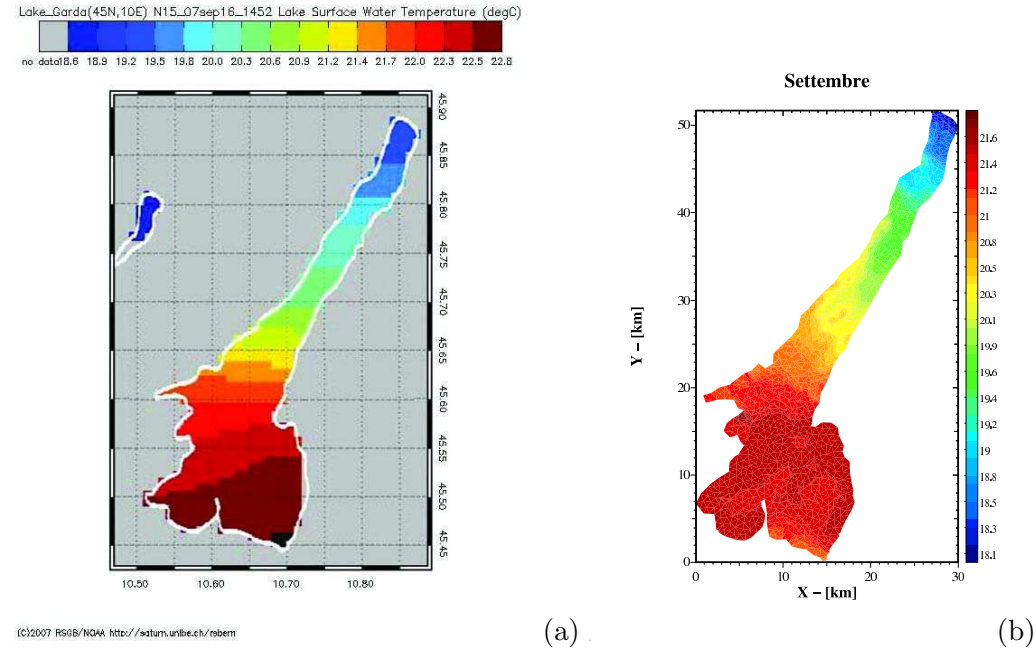

(a) (b)

Figure 3: Water temperature at the surface in a typical September day: (a) remote sensing measurement from NOAA satellite (b) numerically simulated temperature.

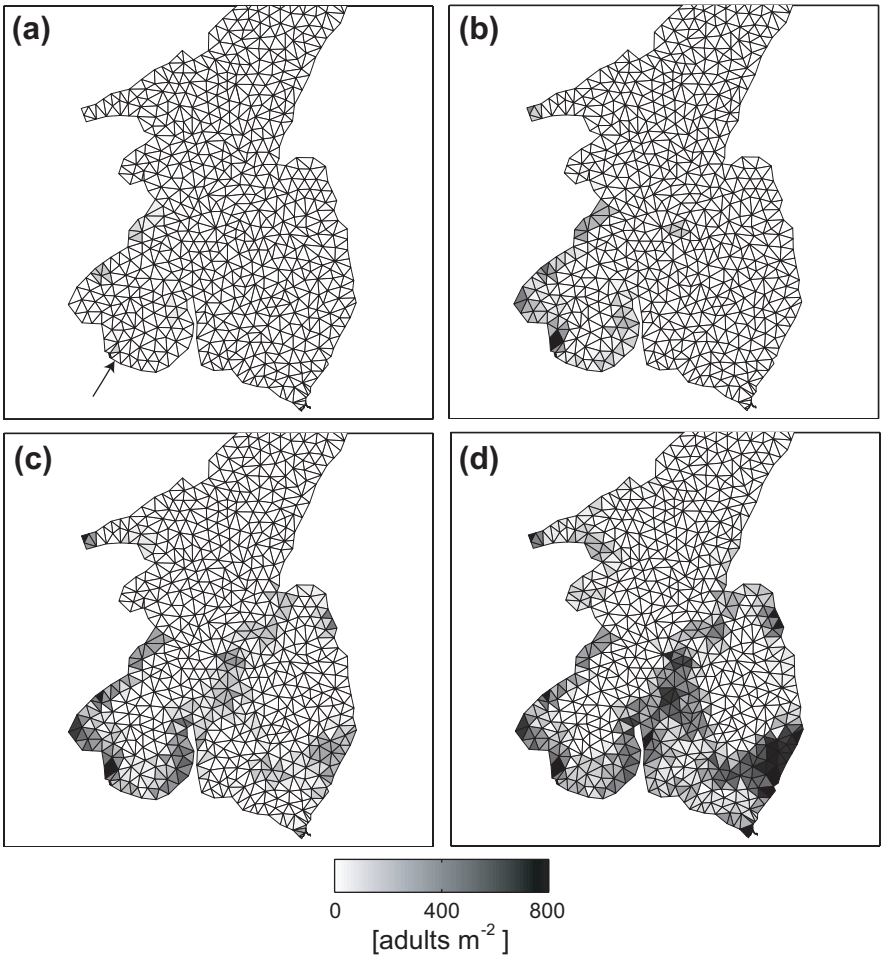

Figure 4: Model simulation results: the abundance of adult individuals is displayed 5 (a), 10 (b), 15 (c) and 20 years (d) after the beginning of the spread. The starting point of the diffusion of the species is marked by the black arrow (Peschiera sul Garda). We limit the plot to the south basin of Lake Garda because it contains most of the viable patches. Model parameters are as in Table 1.

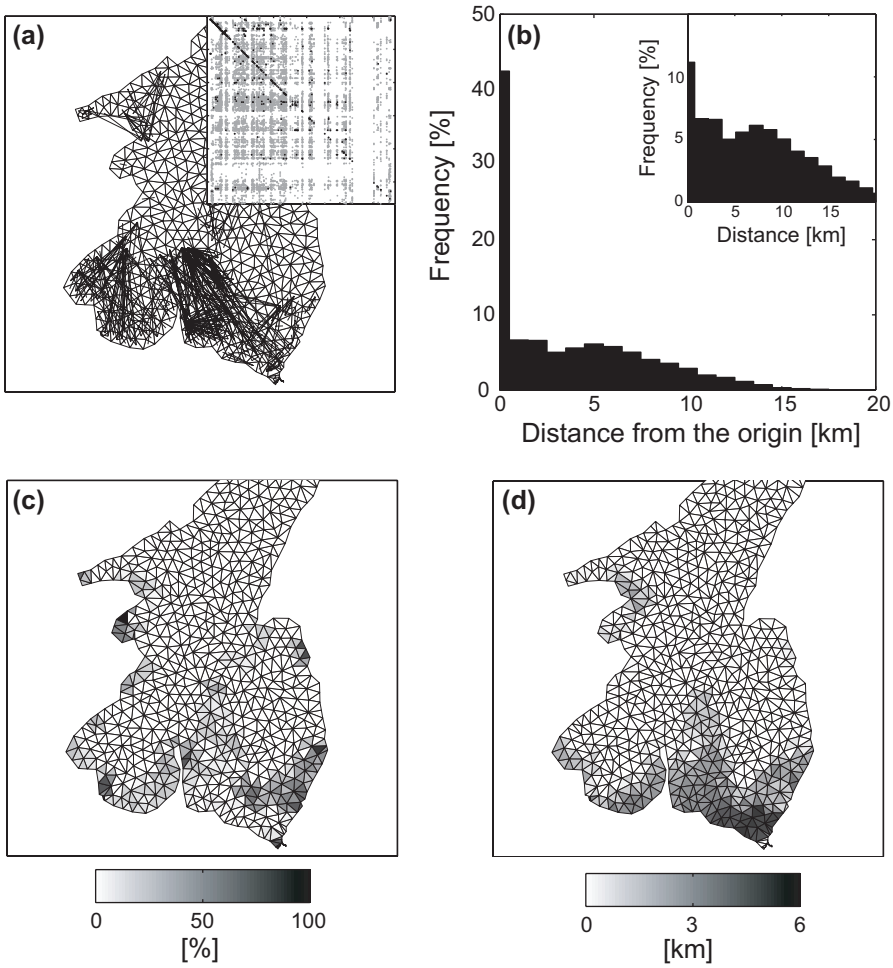

Figure 5: Structure of larval connectivity patterns for the simulation reported in Figure 4. Panel (a) displays connectivity matrix C (inset). The strongest connections ($c_{ij} > 0.05$) are displayed as black dots and are also reported as links between nodes in the geographic layout shown in the main panel. Panel (b) reports the mean dispersal kernel. Inset: dispersal kernel obtained by excluding the effects of self-recruitment. Panel (c) and (d) show self-recruitment and the mean distance traveled by single larvae departing from each viable patch, respectively.

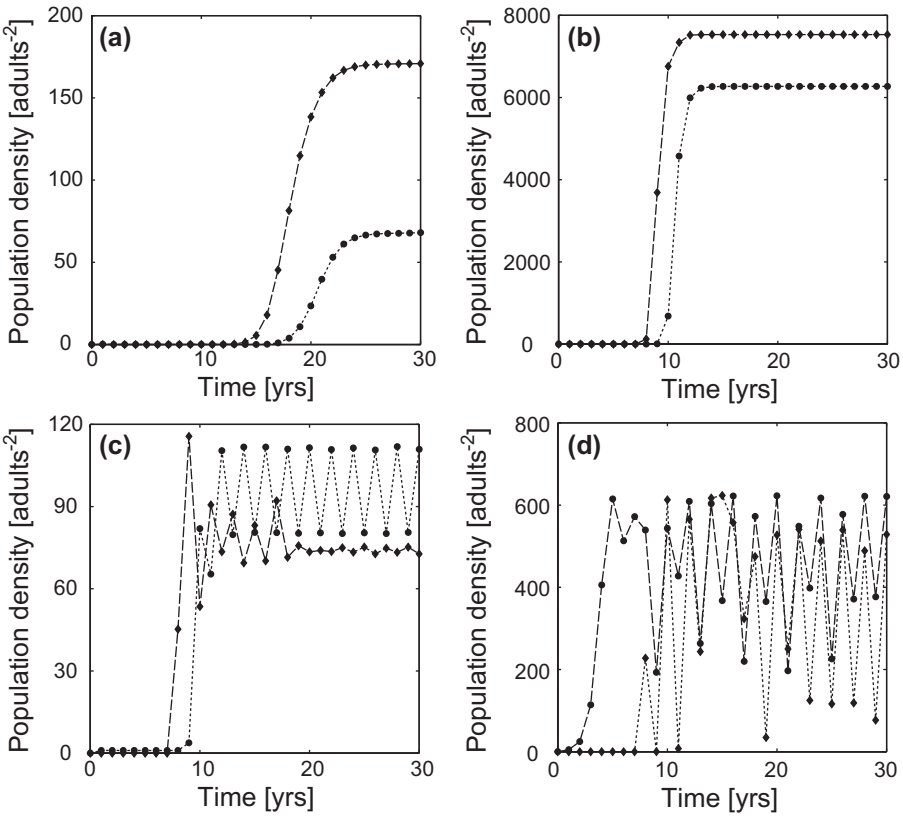

Figure 6: Sensitivity analysis: the role of demographic parameters on local population dynamics. Black dots and diamonds correspond to adult density in Desenzano sul Garda and Bardolino, respectively (see Figure 1). a) $\sigma_0 = 0.01$, $\xi = 1$ (as in Figure 4); b) $\sigma_0 = 0.1$; c) $\sigma_0 = 0.1$, $\xi = 30$; d) $\sigma_0 = 0.5$, $\xi = 30$. Unspecified parameters as in Table 1.

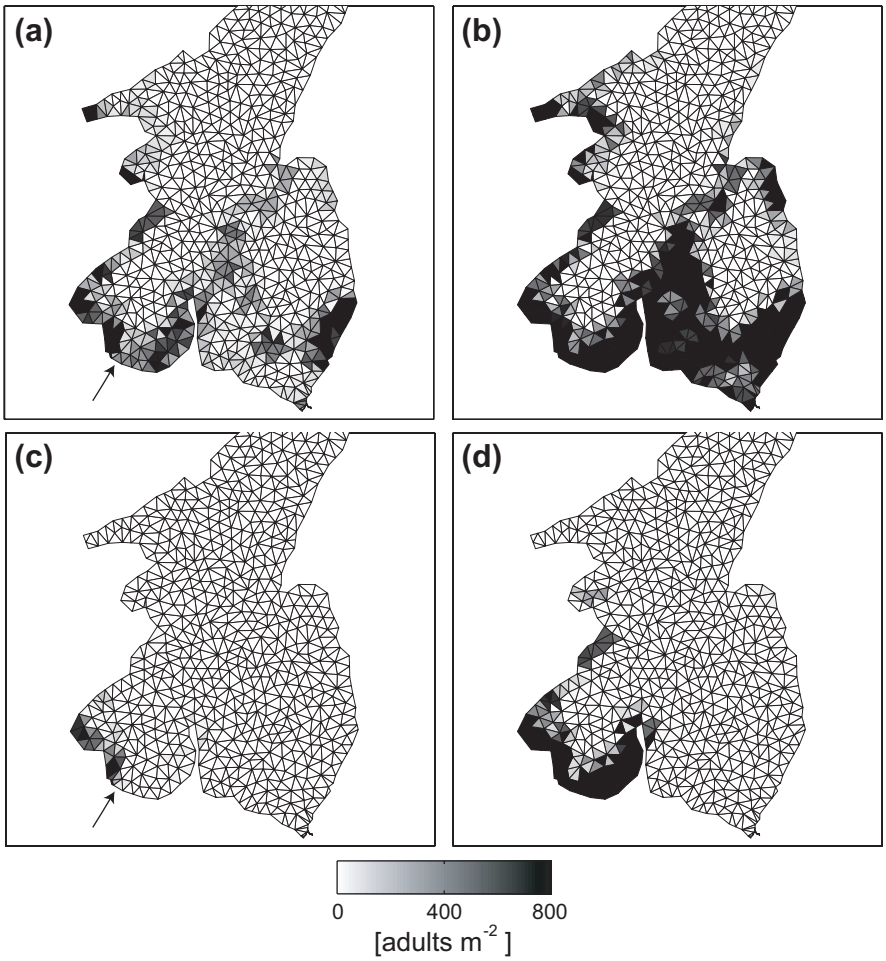

Figure 7: Sensitivity analysis: the role of larval density on the spatiotemporal patterns of population abundance. Top panels: as in Figure 4, with $\rho_L = 1.001\rho$. The abundance of adult individuals is displayed 10 (a) and 20 years (b) after the beginning of the spread. Bottom panels: as in top panels, with $\rho_L = 1.01\rho$. The abundance of adult individuals is displayed 5 (c), and 10 years (d) after the beginning of the spread. The starting point of the diffusion of the species ismarked by the black arrows (Peschiera sul Garda).

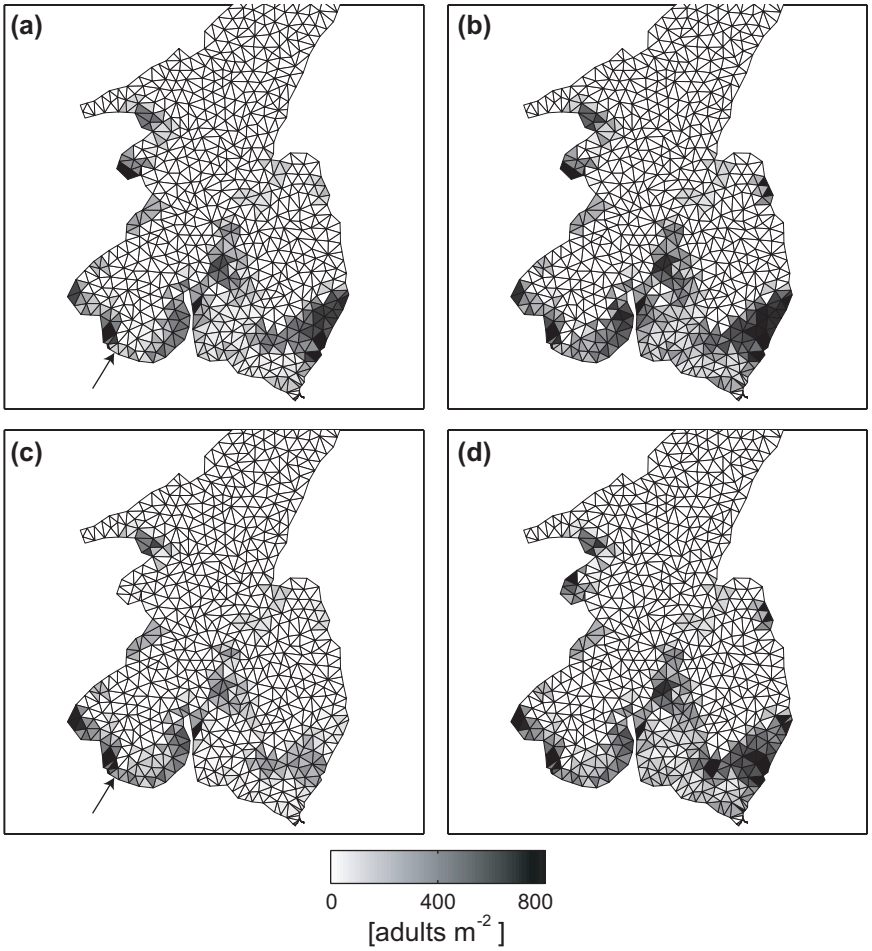

Figure 8: Sensitivity analysis: the role of temperature on the spatiotemporal patterns of population density. Top panels: as in Figure 4, with $T_{min} = 10$ C. The abundance of adult individuals is displayed 15 (a) and 20 years (b) after the beginning of the spread. Bottom panels: as in top panels, with mean and maximum temperatures used in thermal forcing terms increased by 2 C. The abundance of adult individuals is displayed 15 (c) and 20 years (d) after the beginning of the spread. The starting point of the diffusion of the species is marked by the black arrows (Peschiera sul Garda).

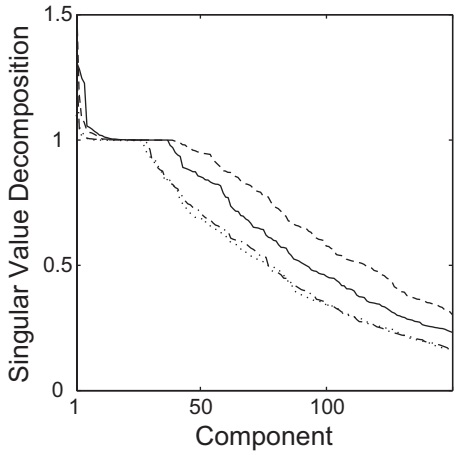

Figure 9: First 150 singular values of the connectivity matrices computed in the cases of Figure 4 (solid line), Figure 7(a-b) (dashed line), Figure 8(a-b) (dash-dotted line) and Figure 8(c-d) (dotted line), respectively.

MOX Technical Reports, last issues

Dipartimento di Matematica "F. Brioschi",
Politecnico di Milano, Via Bonardi 9 - 20133 Milano (Italy)

02/2009 L. Bonaventura, C. Biotto, A. Decoene, L. Mari, E. Miglio:
A couple ecological-hydrodynamic model for the spatial distribution of sessile aquatic species in thermally forced basins

01/2009 E. Miglio, C. Sgarra:
A Finite Element Framework for Option Pricing the Bates Model

28/2008 C. D'Angelo, A. Quarteroni:
On the coupling of 1D and 3D diffusion-reaction equations. Applications to tissue perfusion problems

27/2008 A. Quarteroni:
Mathematical Models in Science and Engineering

26/2008 G. Aletti, C. May, P. Secchi:
A Central Limit Theorem, and related results, for a two-randomly reinforced urn

25/2008 D. Detomi, N. Parolini, A. Quarteroni:
Mathematics in the wind

24/2008 V. Bacchelli, A. Veneziani, S. Vessella:
Corrosion detection in a 2D domain with a polygonal boundary

23/2008 S. Hysing, S Turek, D. Kuzmin, N. Parolini, E. Burman, S. Ganesan, L. Tobiska:
Quantitative benchmark computations of two-dimensional bubble dynamics

22/2008 F. Nobile, R. Tempone:
Analysis and implementation issues for the numerical approximation of parabolic equations with random coefficients

21/2008 P. Antonietti, E. Süli:
Domain Decomposition Preconditioning for Discontinuous Galerkin Approximations of Convection-Diffusion Problems